Time-Resolved Cryo-TEM Study on the Formation of Iron Hydroxides in a Collagen Matrix

Bernette M. Oosterlaken, Mark M. J. van Rijt, Rick R. M. Joosten, Paul H. H. Bomans, Heiner Friedrich, and Gijsbertus de With*

Read Online

ACCESS | Metrics & More | Article Recommendations | Supporting Information

ABSTRACT: The mineralization of collagen via synthetic procedures has been extensively investigated for hydroxyapatite as well as for silica and calcium carbonate. From a fundamental point of view, it is interesting to investigate whether collagen could serve as a generic mineralization template for other minerals, like iron oxides. Here, bio-inspired coprecipitation reaction, generally leading to the formation of magnetite, is used to mineralize collagen with iron hydroxides. Platelet-shaped green rust crystals form outside the collagen matrix, while inside the collagen, nanoparticles with a size of 2.6 nm are formed, which are hypothesized to be iron (III) hydroxide. Mineralization with nanoparticles inside the collagen solely occurs in the presence of poly(aspartic acid) (pAsp). In the absence of pAsp, magnetite particles are formed around the collagen. Time-resolved cryo-TEM shows that during the coprecipitation reaction, initially a beam-sensitive phase is formed, possibly an Fe^{3+}−pAsp complex. This beam-sensitive phase transforms into nanoparticles. In a later stage, sheet-like crystals are also found. After 48 h of mineralization, ordering of the nanoparticles around one of the collagen sub-bands (the a-band) is observed. This is very similar to the collagen−hydroxyapatite system, indicating that mineralization with iron hydroxides inside collagen is possible and proceeds via a similar mechanism as hydroxyapatite mineralization.

KEYWORDS: Iron hydroxides, collagen, electron tomography, biomineralization
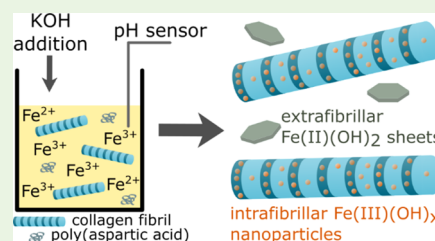
1. INTRODUCTION

Collagen is one of the most abundant proteins in nature. Together with chitin and chitin-like molecules, it is one of the most common templates for the formation of skeletal elements. To this extent, collagen is mineralized with hydroxyapatite in the bone and teeth of vertebrates.[1,2] Mimicking the process of bone formation in vitro, collagen can be mineralized with hydroxyapatite in the presence of an acidic (bio)polymer, like poly(aspartic acid) (pAsp).[3,4]

When imaged using TEM, collagen exhibits a characteristic banding pattern of lighter and darker bands, corresponding to the gap and overlap regions, respectively, which arise from the staggered arrangement of the amino acid triple helices. Additional sub-bands can be visualized via chemical staining with phosphotungstic acid.[5] Following the mineralization reaction with hydroxyapatite with time-resolved cryo-TEM showed that an amorphous precursor infiltrates into the collagen fibril at one of these staining bands, the a-band, before conversion to crystalline platelets.[6]

Minerals other than hydroxyapatite have been used to mineralize collagen. For example, calcium carbonate,[7−10] silica,[11] non-natural yttria-stabilized zirconia,[12] and lepidocrocite (γ-FeOOH)[13] have been infiltrated into fibrillar collagen. However, although these minerals are oriented similar to hydroxyapatite platelets inside the collagen, these minerals display some discrepancies with respect to hydroxyapatite

mineralization inside the collagen. For mineralization with $CaCO_3$, a distortion in the collagen structure is present which is not observed for other minerals. Silica and yttria-stabilized zirconia can only be obtained as a crystalline material after sintering and thus removal of the collagen template, while it appeared that lepidocrocite mineralization was only observed in the outer ∼25 nm of the collagen fibril and not in the central regions of the fibril (see Discussion). Furthermore, although collagen has been investigated as a template for these minerals, these studies have not investigated whether mineralization of collagen with these minerals proceeds via a similar mechanism as for hydroxyapatite.

Time-resolved mechanistic studies with minerals other than hydroxyapatite could indicate whether collagen mineralization proceeds via a generic pathway or via different mechanisms for different minerals. Thus, from a fundamental point of view, it is interesting to investigate whether collagen could serve as a generic template for other (bio)minerals. A particularly appealing (bio)mineral is magnetite due to its magnetic
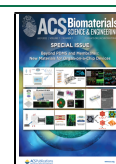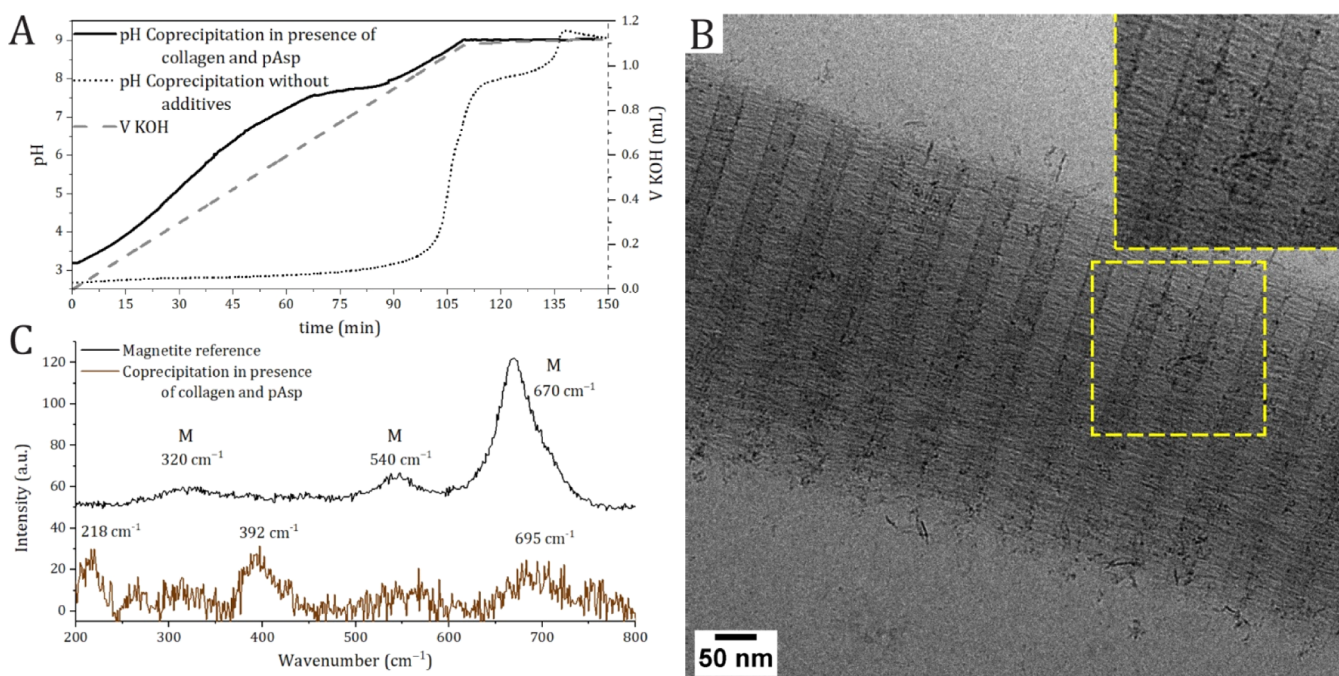
Figure 1. Coprecipitation performed in the presence of collagen and pAsp. (A) pH curve of the reaction performed in the presence of collagen and pAsp (solid line) upon the continuous addition of KOH as a base (dashed line). The pH curve for coprecipitation without additives at the same base addition rate (dotted line) is added as a reference. (B) Cryo-TEM image of the product of the coprecipitation reaction after aging the sample for 8 weeks. (C) Part of the Raman spectra of the product of the coprecipitation (brown), plotted against a magnetite reference (black). Peaks assigned with "M" indicate the magnetite peaks. The peaks at 218 and 392 cm^{-1} could match δ'-FeOOH, which is probably an oxidation product of Fe(OH)$_2$ or green rust (GR).

properties and its hardness.[14] Applications of magnetite include water purification,[15,16] targeted drug delivery,[17,18] and hyperthermia cancer treatment.[19,20] Furthermore, collagen—magnetite hybrid materials are promising for bone cancer treatment.[21,22]

Magnetite, as well as its precursor ferrihydrite and other iron oxide species like goethite or lepidocrocite, is found biologically in, for example, magnetotactic bacteria,[23−26] chitons,[27−31] and limpets.[32,33] In these organisms, the formation of magnetite is precisely regulated, even at ambient temperatures and in aqueous media. Synthetically, magnetite can be formed in water at room temperature via a so-called bioinspired coprecipitation reaction.[34] Acidic polypeptides, mimicking the role of magnetosome proteins in magnetotactic bacteria, are known to influence the nucleation and growth of magnetite crystals during the coprecipitation.[35] Moreover, acidic polypeptides, like pAsp or poly(acrylic acid), were found to promote intrafibrillar mineralization of collagen with hydroxyapatite.[3,36]

Here, we aim to mineralize collagen with magnetite by performing the coprecipitation reaction in the presence of collagen fibrils and pAsp. However, surprisingly, the result of the reaction is nanoparticles and platelet-shaped crystals, which were both identified as iron hydroxides. To gain a better understanding of the pathways involved in the mineralization of collagen with iron hydroxides, the intermediates and products formed during synthesis are analyzed with time-resolved cryo-TEM and cryo-electron tomography (cryo-ET).

2. MATERIALS AND METHODS

2.1. Materials. Ferrous chloride tetrahydrate (FeCl$_2$·4H$_2$O), ferric chloride hexahydrate (FeCl$_3$·6H$_2$O), potassium hydroxide pellets, and pAsp [poly-(α,β)-DL-aspartic acid sodium salt, M_w 2000−11,000]

were purchased from Sigma Aldrich. Resorbable collagen tapes (RCT resorbable collagen tape, 2.5 × 7.5 cm^2, Bovine Collagen type I) were acquired from Henry Schein Dental. All reagents were used without further purification. The collagen tapes were crushed under liquid nitrogen before use. MilliQ water was deaerated under argon flow for at least 1 h and subsequently under nitrogen flow for another 15 min. All solutions and dispersions were prepared using deaerated MilliQ water.

2.2. Coprecipitation Experiments. Coprecipitation experiments were performed in a wet MBraun MB 200B glovebox under a nitrogen atmosphere [(O$_2$) < 5 ppm]. Titration experiments were performed at room temperature with a Metrohm Titrando 901 automated titration setup, controlled by a computer running software program Tiamo 2.5, and equipped with a glass pH electrode (Metrohm article number 6.0234.100) and a Dosino 10 mL dosing device. A solution of ferric chloride (4 mM) and ferrous chloride (2 mM) was titrated with 0.07 M KOH at a rate of 0.01 mL min^{-1} until pH 9 was reached. For experiments in the presence of pAsp, 7 mg mL^{-1} pAsp (12 mM aspartic acid groups) was added to the iron solution. For experiments in the presence of dispersed collagen, the iron solution was added to the collagen to reach a final collagen concentration of 5 mg mL^{-1}.

2.3. Cryo-TEM Analysis. Cryo-TEM analysis was performed on 200 mesh gold support holey carbon grids. The TEM grids were surface plasma treated for 40 s using a Cressington 208 carbon coater prior to use. Three μL of the sample was applied to a TEM grid and blotted for 3.5 s in an automated vitrification robot (Thermo Fisher Scientific Vitrobot Mark III). As it is important to prevent oxidation of the intermediates and/or products during cryo-TEM sample preparation and analysis, the Vitrobot is directly connected to the wet MBraun glovebox. Both glovebox and Vitrobot were customized with an airlock and flange, respectively, which allows direct access between the glovebox and vitrification chamber (Supporting Information Section 1, Figure S1.1). Cryo-TEM imaging was performed on a TU/e cryoTITAN transmission electron microscope (Thermo Fisher Scientific; www.cryotem.nl) operated at 300 kV and equipped with a
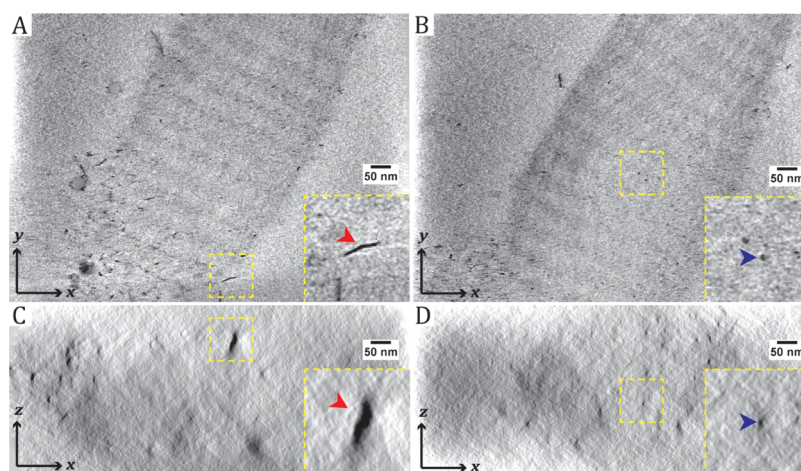
Figure 2. Cryo-ET results of collagen fibrils mineralized via the coprecipitation reaction after aging for 8 weeks. (A,B) Numerical cross section (thickness: 2.9 nm) through the 3D cryo-ET reconstruction along the xy plane. (C,D) Numerical cross section (thickness: 2.9 nm) through the 3D cryo-ET reconstruction along the xz plane, corresponding to images A and B, respectively. Insets: the magnified image of the particles in the 3D-reconstructed volume. The arrows indicate the same particle in both slices. The images are averaged over three slices to reduce noise.

field emission gun, a post-column Gatan 2002 Energy Filter (GIF), and a post-GIF 2k × 2k Gatan model 794 CCD camera.

2.4. TEM Analysis. For TEM analysis, the samples were washed by spin concentrating the sample at 14,500 rpm for 45 s, removing the supernatant and adding fresh deaerated MilliQ water to the sample. This was repeated three times in total. The TEM grids and continuous carbon 200 mesh gold support were surface plasma treated for 40 s using the Cressington 208 carbon coater prior to use. After washing, 20 μL of the sample was deposited on a TEM grid and left to dry on a filter paper inside the wet MBraun glovebox under a nitrogen atmosphere. TEM imaging was performed on Tecnai T20 G2 (Thermo Fisher Scientific), operating at 200 kV and equipped with a LaB$_6$ filament. The images were acquired on a 4k × 4k CETA CMOS camera (Thermo Fisher Scientific).

2.5. Raman Spectroscopy. For Raman spectroscopy, the samples were washed by spin concentrating the sample at 14,500 rpm for 45 s, removing the supernatant and adding fresh deaerated MilliQ water to the sample. This was repeated three times in total. Finally, the samples were spin concentrated at 14,500 rpm for 45 s and the supernatant was removed. Then, 20 μL of the sample was deposited on a glass slide which was covered with aluminum foil. The samples were measured on a WiTec Alpha 300R Raman spectroscope with a 532 nm laser at a laser power of 1 mW. The samples were measured for 30 s during 10 integrations. All acquired spectra were processed (cosmic ray removal and baseline correction) using WiTec Project FIVE 5.1 software.

2.6. Cryo-ET. For cryo-ET, cryo-TEM samples were prepared as described above with 20 nm diameter Au fiducials to facilitate alignment of the tilt series. The cryo-ET series was collected in low-dose mode between −66 and +66° using 2° increments for the 48 h sample and using 3° increments for the 8 week sample. The total electron dose for tilt series acquisition was 135 e$^-$ Å^{-2}, which was well below the maximum dose limit for these samples (Supporting Information Section 2, Figure S2.1). The tilt series was acquired using Inspect3D software (Thermo Fisher Scientific) and aligned and reconstructed using IMOD software using the simultaneous iterative reconstructive technique algorithm.

2.7. Particle Size Analysis. Particle size analysis was performed with an in-house Matlab script. The particle diameters are estimated based on at least 42 measurements in two or more representative TEM images.

The *volume fraction* of nanoparticles inside the collagen was determined via ImageJ. The image was converted to a binary image. The particle analysis plug-in in ImageJ was used to calculate the area %, which is a nonbiased estimate for the vol %.

3. RESULTS

3.1. Mineralization of Collagen with Iron Hydroxides.

Mineralization of collagen with iron hydroxides was performed via bio-inspired coprecipitation reaction, which will be termed coprecipitation hereafter. Briefly, coprecipitation was performed by continuously adding a base to a 1:2 mixture of Fe^{2+} and Fe^{3+} ions in water, in the presence of collagen, while monitoring the pH (Figure 1A). To promote intrafibrillar mineralization, pAsp was added. The reaction was stopped when pH 9 was reached. After aging the sample for 8 weeks, the sample was analyzed using cryo-TEM (Figure 1B) and Raman spectroscopy (Figure 1C).

Upon the continuous addition of potassium hydroxide as a base (Figure 1A, dashed line), the pH gradually increases in the first 70 min of the coprecipitation reaction (Figure 1A, solid line). Then, a plateau is reached at about pH 7.5 (10 min), after which the pH increases again to the set value of 9. This is different from coprecipitation without additives (Figure 1A, dotted line). Whereas the reaction in the presence of collagen and pAsp increases the pH almost instantaneously, the reaction without additives remains at a plateau at about pH 2.7 during the first 100 min of the reaction time. This plateau is generally associated with the precipitation of Fe^{3+} during the formation of ferrihydrite,[34] and the absence of a plateau could indicate that Fe^{3+} is binding to collagen and/or pAsp (see also Supporting Information S1). The collagen does not suffer from damage due to the low pH, as described in Supporting Information Section 1 (Figure S1.2).

Cryo-TEM analysis of the product of the coprecipitation reaction after aging for 8 weeks shows that collagen fibrils are present as well as nanometer-sized particles and needle-shaped crystals, which were identified as green rust (Fe$_x^{II}$Fe$_y^{III}$OH$_{2x+3y-z}$Cl$_z$) using selected area electron diffraction (SAED) on a dried TEM sample (Supporting Information Section 1, Figure S1.3). GR could have formed under the given reaction conditions, but as the SAED was recorded on a dried TEM sample, oxidation of Fe(OH)$_2$ into GR upon exposure to air would also be possible. Raman spectroscopy did not provide a definite answer, as the Raman spectrum points toward the formation of δ'-FeOOH, which most likely is an oxidation product of Fe(OH)$_2$ or GR.
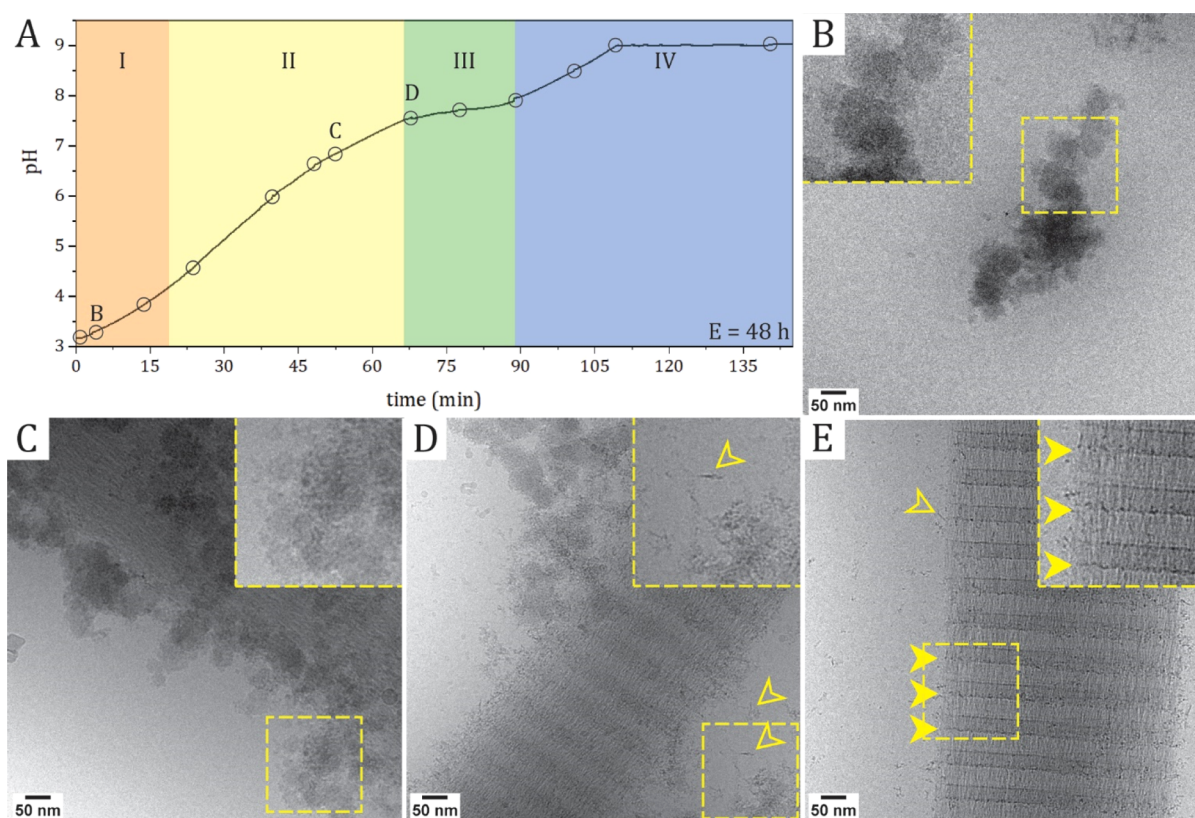
Figure 3. Cryo-TEM sampling during the coprecipitation reaction in the presence of collagen and pAsp. (A) pH curve of the coprecipitation. The circles indicate the time points where samples for cryo-TEM were taken, and the regions indicated are based on cryo-TEM observations. (B–E) Cryo-TEM images of the regions indicated in A. (B) Beam-sensitive material. The collagen fibrils are not in view but are present in the sample. (C) Collagen fibril with beam-sensitive material and nanometer-sized particles. (D) Collagen fibril with sheet-like crystals (open arrows), as well as beam-sensitive material and nanoparticles. (E) Collagen fibril with nanoparticles ordered around the a-bands (closed arrows) and sheet-like crystals (open arrow) after aging the sample for 48 h.

Not only the evolution of pH differs between the coprecipitation reactions but also the products vary. Performing coprecipitation in the absence of additives results in the formation of magnetite (Supporting Information Section 1, Figure S1.4). In a reaction without pAsp, but with collagen, magnetite crystals covering the collagen fibrils are observed (Supporting Information Section 1, Figure S1.5), illustrating the importance of adding pAsp as a promotor for intrafibrillar mineralization, as is also observed for the intrafibrillar mineralization with other minerals.[3,4,8,13] A reaction with pAsp as the only additive results in the formation of goethite crystals (Supporting Information Section 1, Figure S1.6). Using only Fe^{3+} or Fe^{2+} leads to the formation of nanoparticles or sheet-like crystals, respectively (Supporting Information Section 1, Figures S1.7 and S1.8). The sheet-like crystals were identified as GR. Although SAED can be reliably done in case the nanoparticles are sufficiently separated from other materials present, and the ice layer is really thin, in our samples, neither the particles are sufficiently separated from the collagen nor is the ice layer really thin due to the presence of the collagen. Hence, SAED appeared to be impossible on these nanoparticles.

3.2. Cryo-ET on Collagen Mineralized with Iron Hydroxides. From the 2D projection of the TEM images, it cannot be deduced whether the GR crystals and the nanoparticles are located inside or outside the collagen matrix. Moreover, it is not clear whether these crystals are either needle-shaped or platelet-shaped that are viewed on the edge.

To elaborate on this, cryo-ET was performed on a collagen fibril mineralized for 8 weeks (Figure 2; Supporting Information Section 2, Figure S2.2, and Supplementary Movie S1).

After the 3D reconstruction of the cryo-ET tilt series, it becomes clear that the GR crystals are located outside the collagen and are sheet-like in shape instead of needles (Figure 2A,C). Inside the collagen, however, no sheet-like crystals were observed, and instead, approximately spherical particles were observed to be present throughout the collagen fibril (Figure 2B, Supporting Information Section 2, Figure S2.2). The volume fraction of the nanoparticles inside the collagen was estimated to be 0.43 vol % (Supporting Information Section 3). Although it seems that the majority of the particles are present in the dark bands, this could not be confirmed from the volume fraction measurements. Some of the intrafibrillar particles appear elongated due to the limited tilt range and residual misalignments. A discussion on the smallest detectable object size based on the contrast transfer function, voxel size, reconstruction filter, and alignment error considerations is provided in Supporting Information Section 2 to show that the particles fall within the interpretable range. This is also applicable to the cryo-ET on a 48 h mineralized sample, which is discussed in Section 3.4.

3.3. Mechanism Behind Mineralization of Collagen with Iron Hydroxides. To elaborate on the mechanism behind intrafibrillar mineralization with the nanoparticles as observed in cryo-ET, time-resolved cryo-TEM was performed.
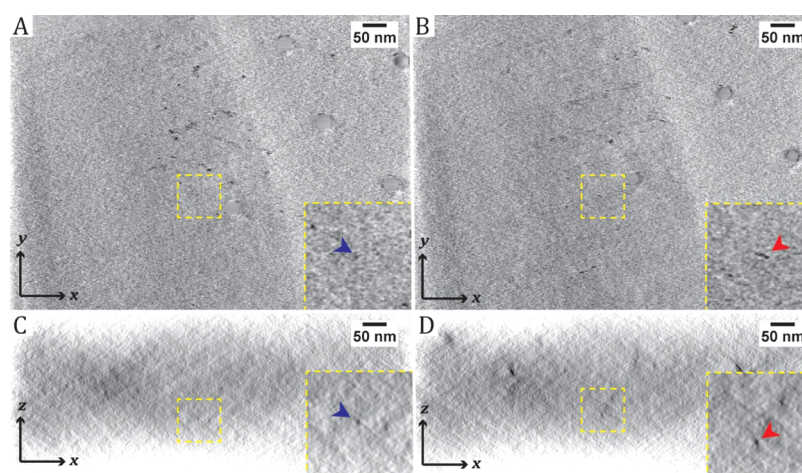
Figure 4. Cryo-ET results of collagen fibrils mineralized via the coprecipitation reaction for 48 h. (A,B) Numerical cross section (thickness: 2.3 nm) through the 3D cryo-ET reconstruction along the *xy* plane. (C,D) Numerical cross section (thickness: 2.3 nm) through the 3D cryo-ET reconstruction along the *xz* plane, corresponding to images A and B, respectively. Insets: the magnified image of nanoparticles in the 3D-reconstructed volume. The arrows indicate the same nanoparticle in both slices. The images are averaged over three slices to reduce noise.

At different time intervals, indicated with a circle in Figure 3A, a sample was taken for cryo-TEM. Based on the time-resolved cryo-TEM analysis, four different regimes, correlating with the evolution of pH, could be identified during the coprecipitation reaction. These regimes are also indicated in Figure 3A, whereas Figure 3B−E shows a representative image for each region.

In the early stages of the reaction (regime I, 0−15 min reaction time), a highly beam-sensitive phase is formed, close to the collagen and in the bulk of the sample. SAED yielded no reliable results. After SAED, these structures were clearly beam-damaged, as could be observed from "bubbles" appearing, even after short exposure times (1 s). The higher magnification images were difficult to obtain due to the beam-sensitivity of the material. Although it seems that clouds of smaller particles are present as shown in Figure 3B, this is not the case. Despite the fact that ferrihydrite, a known product of the early stages of the coprecipitation reaction,[34] is known to be prone to electron-induced degradation,[37] the morphology does not match. We hypothesize that a polymer−iron complex is formed during the early stages of the reaction, which could also explain the beam-sensitivity of the material.

Upon the continued rise in pH (regime II, 15−70 min reaction time), the beam-sensitive phase seems to transform into aggregates, in which individual nanoparticles can be resolved (Figure 3C). These aggregates are typically observed close to the collagen and are no longer beam-sensitive. Next to the beam-sensitive phase and the aggregates, randomly distributed nanoparticles are present. The particles inside the aggregates are 2.9 ± 0.6 nm in diameter, while the particles surrounding the collagen are slightly larger with a diameter of 3.2 ± 0.5 nm (± indicates sample standard deviation, Supporting Information Section 4). Due to this small size with respect to the bulk, it was not possible to identify these nanoparticles with SAED.

In the third regime (70−90 min reaction time), corresponding to a plateau in the pH curve at about pH 7.5, the formation of sheet-like crystals was observed (Figure 3D). Using SAED on a dried TEM sample, these crystals were identified as GR. The beam-sensitive material and the nanometer-sized particles are still present in this regime. As the reaction reached pH 9

(regime IV; > 90 min reaction time), the beam-sensitive material disappeared. Although aggregates of the nanoparticles were no longer observed, the nanoparticles are still present in two populations: in the bulk of the sample and close to the collagen fibril. With a diameter of 2.8 ± 0.6 nm, the nanoparticles in the bulk are comparable in size with the nanoparticles in the aggregates observed in region II. The particles surrounding the collagen, however, decreased in size, to 2.6 ± 0.6 nm (statistically significant at 5% significance level, details in Supporting Information Section 4). The sheet-like GR is still present in regime IV.

As the reaction progresses in time after regime IV, the nanoparticles form ordered arrays around the collagen. This ordering of the nanoparticles seems to occur around one of the bands of the collagen specifically and is most pronounced after aging the sample for 48 h (Figure 3E). Earlier observations for hydroxyapatite mineralization of collagen indicate that a similar array of nanoparticles is formed around one of the collagen staining bands,[6] known as the a-band, a highly charged region at the gap−overlap interface.[5]

From the 2D TEM images, it is impossible to conclude whether the nanometer-sized particles are inside or outside the collagen fibrils. Therefore, we performed 3D cryo-ET on a sample aged for 48 h, which had the most pronounced ordering of nanoparticles around the collagen (Figure 4, Supporting Information Section 2, Figure S2.5, and Supplementary Movie S2).

Figure 3E shows that most of the nanoparticles are observed near the gap−overlap interface. The cryo-ET reconstruction confirms that these nanoparticles are present throughout the thickness of the fibril, indicating that intrafibrillar nanoparticles form already during the early stages of the mineralization.

4. DISCUSSION

This work investigates the growth of iron hydroxides inside and outside a collagen matrix using bio-inspired coprecipitation reaction. During this reaction, the pH is precisely monitored, as described in Section 3.1. In the absence or presence of collagen and/or pAsp, the pH evolves differently. In the reaction without additives, the pH evolves into a plateau at about pH 2.7 (Supporting Information Section 1, Figure

S1.4). This plateau is generally associated with the formation of ferrihydrite and thus the consumption of Fe^{3+} ions.[34] For the reaction with only collagen and the reaction with only pAsp (Supporting Information Section 1, Figures S1.5 and S1.6) as additives, this plateau is significantly shortened, indicating that both collagen and pAsp are binding Fe^{3+}. From the length of this plateau, the amount of Fe^{3+} binding to collagen or pAsp can be estimated: 30 and 36% of Fe^{3+} are bound to the amino acid residues on the outside of the collagen fibril[5,38,39] or to pAsp, respectively (Supporting Information Section 1). Working in synergy, during the reaction with both collagen and pAsp as additives, the plateau at pH 3 is almost absent, indicating that almost all of Fe^{3+} is bound to collagen and/or pAsp. However, in reaction with only Fe^{3+} present at a slightly higher concentration (Supporting Information Section 1, Figure S1.7), a plateau is observed again. When estimating the amount of Fe^{3+} binding to collagen and/or pAsp, it seems that the same absolute amount of Fe^{3+} binds to the collagen and/or pAsp. This indicates that the reaction described in this paper uses the maximum amount of Fe^{3+} that can be bound to the amount of collagen and/or pAsp present in the system. In reaction with only Fe^{2+} (Supporting Information Section 1, Figure S1.8), the plateau at about pH 3 is completely absent, and the pH of the reaction starts at pH 6.5 already. The interactions between collagen, pAsp, and Fe^{2+} could not be quantified directly, as only the shape of the increase in pH and the pH around which a plateau evolves seem to change, while the length of this second plateau does not significantly change.

The binding of collagen to Fe^{3+} is also indicated by the cryo-TEM images of the products of each of the reactions. In the absence of pAsp, but in the presence of collagen, the bio-inspired coprecipitation reaction leads to the formation of extrafibrillar magnetite crystals. There seems to be some interaction between iron and collagen indeed, as all collagen fibrils are coated with a layer of magnetite particles. Thus, it appears that some of the Fe ions are bound to the collagen, possibly with amino acid residues on the outside of the fibrils. Only when using both collagen and pAsp, intrafibrillar nanoparticles are observed, as shown via cryo-ET (Section 3.2). This indicates that pAsp plays an important role in driving the formation of intrafibrillar nanoparticles. This is very similar to the often investigated hydroxyapatite−collagen system, where pAsp or another charged polymer is deemed crucial for the formation of intrafibrillar hydroxyapatite crystals,[3,4] though its exact role in intrafibrillar mineralization is still poorly understood.

The intrafibrillar nanoparticles are hypothesized to be a product of Fe^{3+}, as they are observed in reactions with Fe^{3+} exclusively. Possibly they are iron hydroxides or even iron oxyhydroxide phases. Unfortunately, these nanoparticles are very small (2−3 nm in size), and due to the collagen that is close to or surrounding the nanoparticles, it was impossible to reduce the background signal in SAED. Moreover, because of the weak signals arising from the nanoparticles, due to their small volume with respect to the bulk, these signals were not observed. Their small size also limits the interaction with (laser) light, resulting in no signal in Raman spectroscopy. Thus, it could not be deduced which iron-containing compound formed during this reaction. Based on the reaction conditions, in which the base is continuously added to the system, the observation that the nanoparticles are only formed in reactions with Fe^{3+} and the fact that oxyhydroxides are

typically an oxidation product of an Fe^{2+} phase,[40] we speculate that these nanoparticles are iron (III) hydroxides. Next to the intrafibrillar nanoparticles, extrafibrillar sheet-like crystals were observed in the cryo-ET. These crystals seem to be an Fe^{2+} compound, as they are observed exclusively in reactions with Fe^{2+}. Diffraction in cryo-TEM yielded no signal. This is possibly due to their small volume with respect to the bulk, hampering the observation of the diffraction signal of the thin crystals. In dry TEM, however, a signal could be observed, which matches GR. GR can be an oxidation product of $Fe(OH)_2$ upon exposure to air but could also have formed under the given reaction conditions. As GR was also observed for reaction with only Fe^{2+} present, performed under very low concentrations of oxygen (<5 ppm), it is assumed that GR is the oxidation product in this case, and thus, $Fe(OH)_2$ is the initial product during the reaction. Thus, although the product could not be unequivocally identified, it does result from the presence of Fe^{2+} ions, which are possibly partially oxidized.

The formation of intrafibrillar nanoparticles is different from the results obtained in studies by Xu et al.[13] Following a similar coprecipitation procedure in the presence of pAsp and collagen, Xu et al. observed the formation of platelet-shaped lepidocrocite (γ-FeOOH) crystals exclusively in the outer ~25 nm of the collagen, for which we estimated the volume fraction as ~1.8 vol % (Supporting Information Section 3). They ascribed the mineralization of the outer regions of the collagen to the limited solubility of Fe^{3+} ions. In contrast, although we do not observe the formation of mature crystals, the Fe^{3+} nanoparticles are found throughout the entire thickness of the fibril, with an estimated volume fraction of ~0.4 vol % (Supporting Information Section 3). Remarkably, with an average fibril diameter of 300 nm in the case of the studies by Xu et al.[13] and 500 nm in our case, the volume fractions referring to the infiltrated material only are approximately three times as high as for our system, while the size of our particles is about half of those reported by Xu et al.[13] Furthermore, although the procedures seem similar at a first glance, there are distinct differences between the experimental procedure reported by Xu et al. and the procedure described here. Xu et al. incubated a solution of pAsp, collagen, $FeCl_3$, and $FeCl_2$ overnight before placing it inside a glovebox.[13] Thus, oxidation of Fe^{2+} might have occurred in their system, as is also indicated by the formation of lepidocrocite, which is typically formed upon oxidation of Fe^{2+} species.[40] Additionally, in the absence of pAsp, they observed the formation of ferrihydrite (an Fe^{3+} compound) around the collagen, whereas we observe the formation of magnetite, consisting of Fe^{2+} and Fe^{3+}. All this indicates that the mineralization system as described by Xu et al. follows a different reaction pathway for the formation of intrafibrillar nanoparticles. The oxidation effects during specimen transfer in air and drying effects due to dehydration of the collagen might have also played a role in their system.

Time-resolved cryo-TEM provides more insights into the processes occurring during the bio-inspired coprecipitation in the presence of collagen and pAsp (Section 3.3). In the early stages of the reaction, a beam-sensitive phase is observed. This phase is suggested to be an Fe−pAsp complex. Almost all beam-sensitive materials are observed covering the collagen. As the pH increases, the formation of nanoparticles is observed, and at the plateau at pH 7.5, the formation of sheet-like crystals starts.

Based on the hydroxyapatite—collagen system, which continuously progresses in time until full mineralization of the fibril is reached, it was expected that the extent of mineralization with iron hydroxides would increase upon aging the sample. However, our observations indicate that aging the iron hydroxide sample for 8 weeks does not result in a significant increase in the mineral content compared to the sample aged for 48 h. Moreover, whereas hydroxyapatite mineralization inside the collagen leads to the formation of long, elongated crystals after a few days of mineralization,[3] such mature crystals were not observed in the iron hydroxide system. Only when aging the dispersion for 400 days (13 months), mature goethite crystals were observed that are aligned with the collagen fibril (Supporting Information Section 2, Figure S2.5). Cryo-ET confirmed that these crystals are not intrafibrillar minerals but are attached to the outside of the collagen fibril instead (Supporting Information Section 2, Figure S2.5).

Remarkably, during the reaction and the aging of the sample, the nanoparticles start to order around one of the collagen staining bands specifically. This band, the a-band, is known as a highly charged region, and previously it was demonstrated that amorphous calcium phosphate infiltrates at the a-band after 48 h mineralization time,[6] after which the fibers become fully mineralized within a few days. Although collagen has been mineralized with other minerals, the onset of nucleation for these minerals has not been investigated. It has been hypothesized by Xu et al. that the onset of mineralization could be similar for non-native minerals,[13] but this has not been confirmed yet. Here, we demonstrate that a similar ordering of the early-stage structures around the a-band occurs after 48 h mineralization time. This indicates that the nucleation sites are indeed the same for hydroxyapatite and iron hydroxides. This is possibly also true for other minerals and suggests that collagen could act as a generic mineralization template. Using cryo-ET on a sample displaying the most pronounced ordering, also after 48 h mineralization time, it was observed that nanoparticles are already present throughout the collagen during this phase. Not only does this indicate that the formation of intrafibrillar structures occurs relatively early during the reaction but also demonstrates that the onset of mineralization is quite similar to that of hydroxyapatite, even though no mature crystals were observed.

5. CONCLUSIONS

Using bio-inspired coprecipitation reaction, we aimed to mineralize collagen with magnetite. pAsp, known to facilitate intrafibrillar mineralization of collagen with hydroxyapatite, was added to promote iron hydroxide mineralization inside the collagen matrix. In this reaction, first a beam-sensitive phase forms, possibly an iron—polymer complex, followed by the formation of nanoparticles. These nanoparticles are an Fe^{3+} phase, most likely iron(III) hydroxide, though its exact nature could not be resolved with certainty, as the nanoparticles are too small with respect to the bulk to produce any reliable signal in electron diffraction or Raman spectroscopy. Lastly, the formation of thin platelet-shaped iron hydroxide crystals was observed, identified as GR, which is hypothesized to be an oxidation product of $Fe(OH)_2$. Under the reaction conditions used here, collagen and pAsp seem to mainly interact with Fe^{3+}, as intrafibrillar structures form as the reaction progresses. These intrafibrillar nanoparticles are found throughout the entire thickness of the collagen fibril, in contrast with previous observations in which γ-FeOOH was observed in the outer 25 nm of the collagen fibrils only. These intrafibrillar structures are formed exclusively in the presence of pAsp, indicating that pAsp is crucial in driving the formation of intrafibrillar structures, similar to the collagen—hydroxyapatite system. Also, the onset of mineralization appears similar, as ordering of intrafibrillar early-stage structures is observed around one of the collagen bands, the a-band, after 48 h mineralization time. This observation was made so far only for hydroxyapatite, where amorphous calcium phosphate enters the collagen at these specific sites. Now, we have confirmed that this is also the case for iron hydroxides. Thus, the mineralization mechanism of iron hydroxides inside collagen appears to be very similar to that of collagen mineralization with hydroxyapatite. This is an indication that collagen indeed could serve as a generic mineralization template, and thus, regardless of the mineral infiltrated into the collagen, all mineralization inside collagen in the presence of a negatively charged polymer occurs via the same mechanism, guided by the amino acid residues on the collagen fibril.

■ ASSOCIATED CONTENT

■ AUTHOR INFORMATION

Corresponding Author

Gijsbertus de With − *Laboratory of Physical Chemistry and Center for Multiscale Electron Microscopy, Department of Chemical Engineering and Chemistry, Eindhoven University of Technology, Eindhoven 5600 MB, The Netherlands;* ⓞ orcid.org/0000-0002-7163-8429; Email: G.deWith@tue.nl

Authors

Bernette M. Oosterlaken − *Laboratory of Physical Chemistry and Center for Multiscale Electron Microscopy, Department of Chemical Engineering and Chemistry, Eindhoven University of Technology, Eindhoven 5600 MB, The Netherlands*

Mark M. J. van Rijt − *Laboratory of Physical Chemistry and Center for Multiscale Electron Microscopy, Department of Chemical Engineering and Chemistry, Eindhoven University of Technology, Eindhoven 5600 MB, The Netherlands;* ⓞ orcid.org/0000-0002-9134-7493

Rick R. M. Joosten − *Laboratory of Physical Chemistry and Center for Multiscale Electron Microscopy, Department of Chemical Engineering and Chemistry, Eindhoven University of Technology, Eindhoven 5600 MB, The Netherlands*

Paul H. H. Bomans − *Laboratory of Physical Chemistry and Center for Multiscale Electron Microscopy, Department of Chemical Engineering and Chemistry, Eindhoven University of Technology, Eindhoven 5600 MB, The Netherlands*

Heiner Friedrich − *Laboratory of Physical Chemistry and Center for Multiscale Electron Microscopy, Department of Chemical Engineering and Chemistry, Eindhoven University*

of Technology, Eindhoven 5600 MB, The Netherlands;
🔘 orcid.org/0000-0003-4582-0064

Complete contact information is available at:
https://pubs.acs.org/10.1021/acsbiomaterials.1c00416

Author Contributions

The manuscript was written through contributions of all authors. All authors have given approval to the final version of the manuscript.

Notes

The authors declare no competing financial interest.

■ ABBREVIATION

3D, three-dimensional; cryo-ET, cryo-electron tomography; cryo-TEM, cryo-transmission electron microscopy; GR, green rust; pAsp, poly(aspartic acid); SAED, selected area electron diffraction; TEM, transmission electron microscopy

■ REFERENCES

(1) Weiner, S.; Traub, W. Organization of hydroxyapatite crystals within collagen fibrils. *FEBS Lett.* **1986**, *206*, 262−266.

(2) Weiner, S.; Veis, A.; Beniash, E.; Arad, T.; Dillon, J. W.; Sabsay, B.; Siddiqui, F. Peritubular Dentin Formation: Crystal Organization and the Macromolecular Constituents in Human Teeth. *J. Struct. Biol.* **1999**, *126*, 27−41.

(3) Olszta, M. J.; Cheng, X. G.; Jee, S. S.; Kumar, R.; Kim, Y. Y.; Kaufman, M. J.; Douglas, E. P.; Gower, L. B. Bone structure and formation: A new perspective. *Mater. Sci. Eng., R* **2007**, *58*, 77−116.

(4) Deshpande, A. S.; Beniash, E. Bioinspired Synthesis of Mineralized Collagen Fibrils. *Cryst. Growth Des.* **2008**, *8*, 3084−3090.

(5) Chapman, J. A.; Tzaphlidou, M.; Meek, K. M.; Kadler, K. E. The collagen fibril-A model system for studying the staining and fixation of a protein. *Electron. Microsc. Rev.* **1990**, *3*, 143−182.

(6) Nudelman, F.; Pieterse, K.; George, A.; Bomans, P. H. H.; Friedrich, H.; Brylka, L. J.; Hilbers, P. A. J.; de With, G.; Sommerdijk, N. A. J. M. The role of collagen in bone apatite formation in the presence of hydroxyapatite nucleation inhibitors. *Nat. Mater.* **2010**, *9*, 1004−1009.

(7) Olszta, M.; Odom, D.; Douglas, E.; Gower, L. A New Paradigm for Biomineral Formation: Mineralization via an Amorphous Liquid-Phase Precursor. *Connect. Tissue Res.* **2003**, *44*, 326−334.

(8) Olszta, M. J.; Douglas, E. P.; Gower, L. B. Scanning electron microscopic analysis of the mineralization of type I collagen via a polymer-induced liquid-precursor (PILP) process. *Calcif. Tissue Int.* **2003**, *72*, 583−591.

(9) Olszta, M. J.; Douglas, E. P.; Gower, L. B. Intrafibrillar mineralization of collagen using a liquid-phase mineral precursor. *Mater. Res. Soc. Symp. Proc.* **2003**, *774*, 127−134.

(10) Ping, H.; Xie, H.; Wan, Y.; Zhang, Z.; Zhang, J.; Xiang, M.; Xie, J.; Wang, H.; Wang, W.; Fu, Z. Confinement controlled mineralization of calcium carbonate within collagen fibrils. *J. Mater. Chem. B* **2016**, *4*, 880−886.

(11) Niu, L.-n.; Jiao, K.; Qi, Y.-p.; Yiu, C. K. Y.; Ryou, H.; Arola, D. D.; Chen, J.-h.; Breschi, L.; Pashley, D. H.; Tay, F. R. Infiltration of Silica Inside Fibrillar Collagen. *Angew. Chem., Int. Ed.* **2011**, *50*, 11688−11691.

(12) Zhou, B.; Niu, L.-n.; Shi, W.; Zhang, W.; Arola, D. D.; Breschi, L.; Mao, J.; Chen, J.-h.; Pashley, D. H.; Tay, F. R. Adopting the principles of collagen biomineralization for intrafibrillar infiltration of yttria-stabilized zirconia into three-dimensional collagen scaffolds. *Adv. Funct. Mater.* **2014**, *24*, 1895−1903.

(13) Xu, Y.; Nudelman, F.; Eren, E. D.; Wirix, M. J. M.; Cantaert, B.; Nijhuis, W. H.; Hermida-Merino, D.; Portale, G.; Bomans, P. H. H.; Ottmann, C.; Friedrich, H.; Bras, W.; Akiva, A.; Orgel, J. P. R. O.; Meldrum, F. C.; Sommerdijk, N. Intermolecular channels direct crystal orientation in mineralized collagen. *Nat. Commun.* **2020**, *11*, 5068.

(14) Mirabello, G.; Lenders, J. J. M.; Sommerdijk, N. A. J. M. Bioinspired synthesis of magnetite nanoparticles. *Chem. Soc. Rev.* **2016**, *45*, 5085−5106.

(15) Wang, P.; Shi, Q.; Shi, Y.; Clark, K. K.; Stucky, G. D.; Keller, A. A. Magnetic Permanently Confined Micelle Arrays for Treating Hydrophobic Organic Compound Contamination. *J. Am. Chem. Soc.* **2009**, *131*, 182−188.

(16) Chandra, V.; Park, J.; Chun, Y.; Lee, J. W.; Hwang, I.-C.; Kim, K. S. Water-Dispersible Magnetite-Reduced Graphene Oxide Composites for Arsenic Removal. *ACS Nano* **2010**, *4*, 3979−3986.

(17) Guo, S.; Li, D.; Zhang, L.; Li, J.; Wang, E. Monodisperse mesoporous superparamagnetic single-crystal magnetite nanoparticles for drug delivery. *Biomaterials* **2009**, *30*, 1881−1889.

(18) Roullin, V.-G.; Deverre, J.-R.; Lemaire, L.; Hindré, F.; Venier-Julienne, M.-C.; Vienet, R.; Benoit, J.-P. Anti-cancer drug diffusion within living rat brain tissue: an experimental study using [3H](6)-5-fluorouracil-loaded PLGA microspheres. *Eur. J. Pharm. Biopharm.* **2002**, *53*, 293−299.

(19) Jordan, A.; Scholz, R.; Wust, P.; Fähling, H.; Roland, F. Magnetic fluid hyperthermia (MFH): Cancer treatment with AC magnetic field induced excitation of biocompatible superparamagnetic nanoparticles. *J. Magn. Magn. Mater.* **1999**, *201*, 413−419.

(20) Jordan, A.; Scholz, R.; Maier-Hauff, K.; Johannsen, M.; Wust, P.; Nadobny, J.; Schirra, H.; Schmidt, H.; Deger, S.; Loening, S.; Lanksch, W.; Felix, R. Presentation of a new magnetic field therapy system for the treatment of human solid tumors with magnetic fluid hyperthermia. *J. Magn. Magn. Mater.* **2001**, *225*, 118−126.

(21) Andronescu, E.; Ficai, M.; Voicu, G.; Ficai, D.; Maganu, M.; Ficai, A. Synthesis and characterization of collagen/hydroxyapatite: magnetite composite material for bone cancer treatment. *J. Mater. Sci.: Mater. Med.* **2010**, *21*, 2237−2242.

(22) Marques, C.; Ferreira, J. M.; Andronescu, E.; Ficai, D.; Sonmez, M.; Ficai, A. Multifunctional materials for bone cancer treatment. *Int. J. Nanomed.* **2014**, *9*, 2713−2725.

(23) Miot, J.; Benzerara, K.; Morin, G.; Kappler, A.; Bernard, S.; Obst, M.; Férard, C.; Skouri-Panet, F.; Guigner, J.-M.; Posth, N.; Galvez, M.; Brown, G. E.; Guyot, F. Iron biomineralization by anaerobic neutrophilic iron-oxidizing bacteria. *Geochim. Cosmochim. Acta* **2009**, *73*, 696−711.

(24) Prozorov, T. Magnetic microbes: Bacterial magnetite biomineralization. *Semin. Cell Dev. Biol.* **2015**, *46*, 36−43.

(25) Frankel, R. B.; Papaefthymiou, G. C.; Blakemore, R. P.; O'Brien, W. Fe3O4 Precipitation in Magnetotactic Bacteria. *Biochim. Biophys. Acta* **1983**, *763*, 147−159.

(26) Fdez-Gubieda, M. L.; Muela, A.; Alonso, J.; García-Prieto, A.; Olivi, L.; Fernández-Pacheco, R.; Barandiarán, J. M. Magnetite Biomineralization in Magnetospirillum gryphiswaldense: Time-Resolved Magnetic and Structural Studies. *ACS Nano* **2013**, *7*, 3297−3305.

(27) Mizota, M.; Maeda, Y. Magnetite in the radular teeth of chitons. *Hyperfine Interact.* **1986**, *29*, 1423−1426.

(28) Han, Y.; Liu, C.; Zhou, D.; Li, F.; Wang, Y.; Han, X. Magnetic and structural properties of magnetite in radular teeth of chiton Acanthochiton rubrolinestus. *Bioelectromagnetics* **2011**, *32*, 226−233.

(29) Kim, K. s.; Macey, D. J.; Webb, J.; Mann, S.; Williams, R. J. P. Iron mineralization in the radula teeth of the chiton Acanthopleura hirtosa. *Proc. R. Soc. London, Ser. B* **1989**, *237*, 335−346.

(30) Gordon, L. M.; Román, J. K.; Everly, R. M.; Cohen, M. J.; Wilker, J. J.; Joester, D. Selective formation of metastable ferrihydrite in the chiton tooth. *Angew. Chem., Int. Ed.* **2014**, *53*, 11506−11509.

(31) Saunders, M.; Kong, C.; Shaw, J. A.; Macey, D. J.; Clode, P. L. Characterization of biominerals in the radula teeth of the chiton, Acanthopleura hirtosa. *J. Struct. Biol.* **2009**, *167*, 55−61.

(32) Mann, S.; Perry, C. C.; Webb, J.; Luke, B.; Williams, R. J. P. Structure, morphology, composition and organization of biogenic minerals in limpet teeth. *Proc. R. Soc. London, Ser. B* **1986**, *227*, 179−190.

(33) Faivre, D.; Godec, T. U. From bacteria to mollusks: the principles underlying the biomineralization of iron oxide materials. *Angew. Chem., Int. Ed.* **2015**, *54*, 4728−4747.

(34) Lenders, J. J. M.; Altan, C. L.; Bomans, P. H. H.; Arakaki, A.; Bucak, S.; de With, G.; Sommerdijk, N. A. J. M. A Bioinspired Coprecipitation Method for the Controlled Synthesis of Magnetite Nanoparticles. *Cryst. Growth Des.* **2014**, *14*, 5561−5568.

(35) Lenders, J. J. M.; Zope, H. R.; Yamagishi, A.; Bomans, P. H. H.; Arakaki, A.; Kros, A.; de With, G.; Sommerdijk, N. A. J. M. Bioinspired Magnetite Crystallization Directed by Random Copoly-peptides. *Adv. Funct. Mater.* **2015**, *25*, 711−719.

(36) Tay, F. R.; Pashley, D. H. Guided tissue remineralisation of partially demineralised human dentine. *Biomaterials* **2008**, *29*, 1127−1137.

(37) Konishi, H.; Xu, H.; Guo, H. In *Nature's Nanostructures*; Barnard, A. S., Guo, H., Eds.; CRC Press, Taylor & Francis Group: Boca Raton, 2012.

(38) Orgel, J.; Perumal, S.; Antipova, O.; Irving, T. The molecular structure and arrangement of collagen type I. *Matrix Biol.* **2006**, *25*, S76.

(39) Oosterlaken, B. M.; Vena, M. P.; de With, G. In Vitro Mineralization of Collagen. *Adv. Mater.* **2021**, *31*, 2004418.

(40) Cornell, R. M.; Schwertmann, U. *The Iron Oxides*; Wiley-VCH Verlag GmbH&Co.: Weinheim, 2003.